Supplement of Atmos. Chem. Phys., 25, 3029–3048, 2025
https://doi.org/10.5194/acp-25-3029-2025-supplement

Atmospheric Chemistry and Physics
Open Access
EGU

Supplement of

Enhanced understanding of atmospheric blocking modulation on ozone dynamics within a high-resolution Earth system model

Wenbin Kou et al.

Correspondence to: Yang Gao (yanggao@ouc.edu.cn)

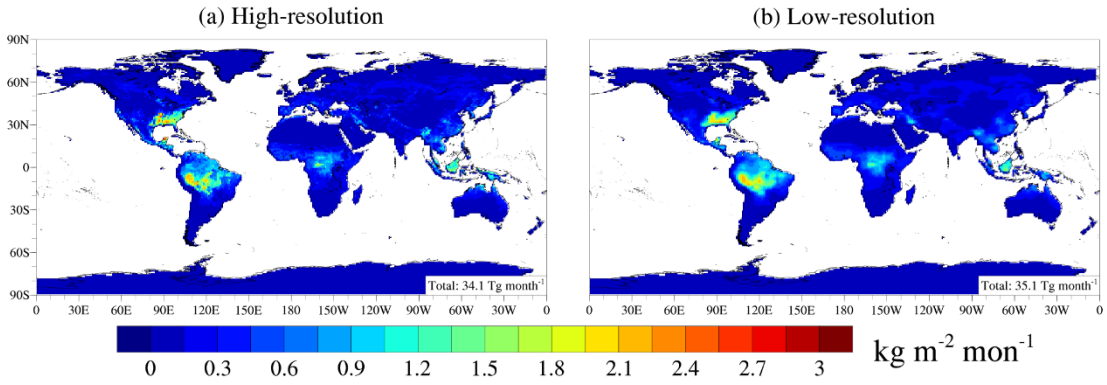

Fig. S1 Spatial distribution of isoprene emissions. Shown are results at high-resolution (0.25°×0.325°) and low-resolution (2°×2.5°) simulations based on Weng et al. (2020).

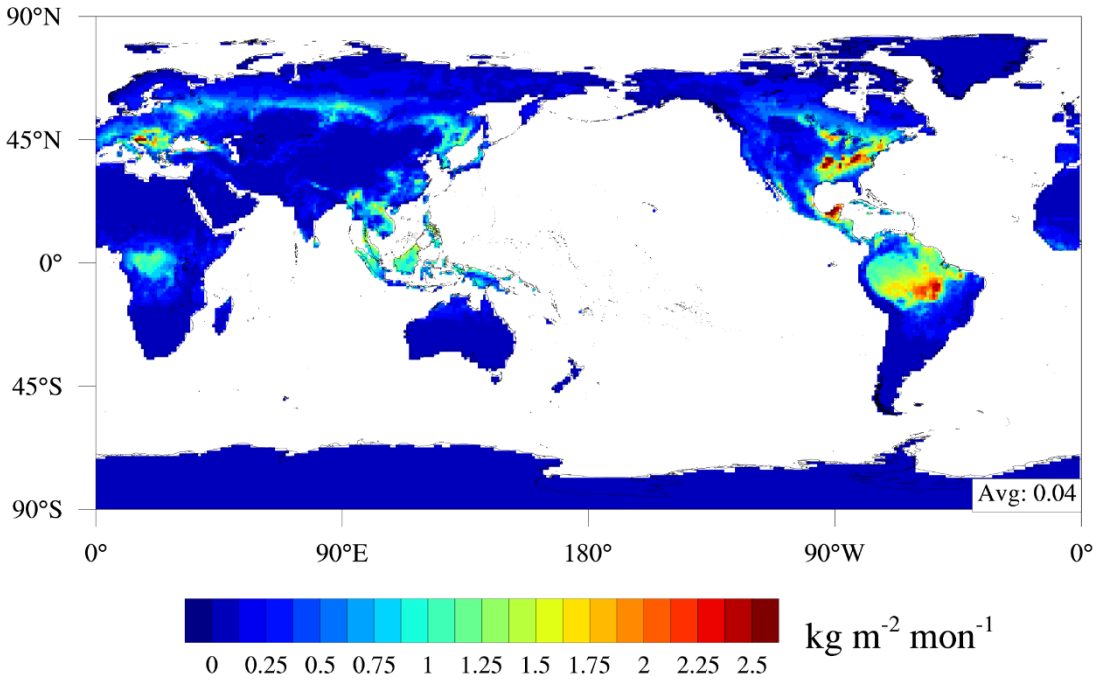

Fig. S2 Spatial distribution of isoprene emission standard deviation in the high-resolution simulations. Shown are results equivalent to the low-resolution grids, with each value representing the standard deviation calculated using the proximately sixteen grids in high-resolution (i.e., 25 km) simulations corresponding to the low-resolution (i.e., 100 km) grid.

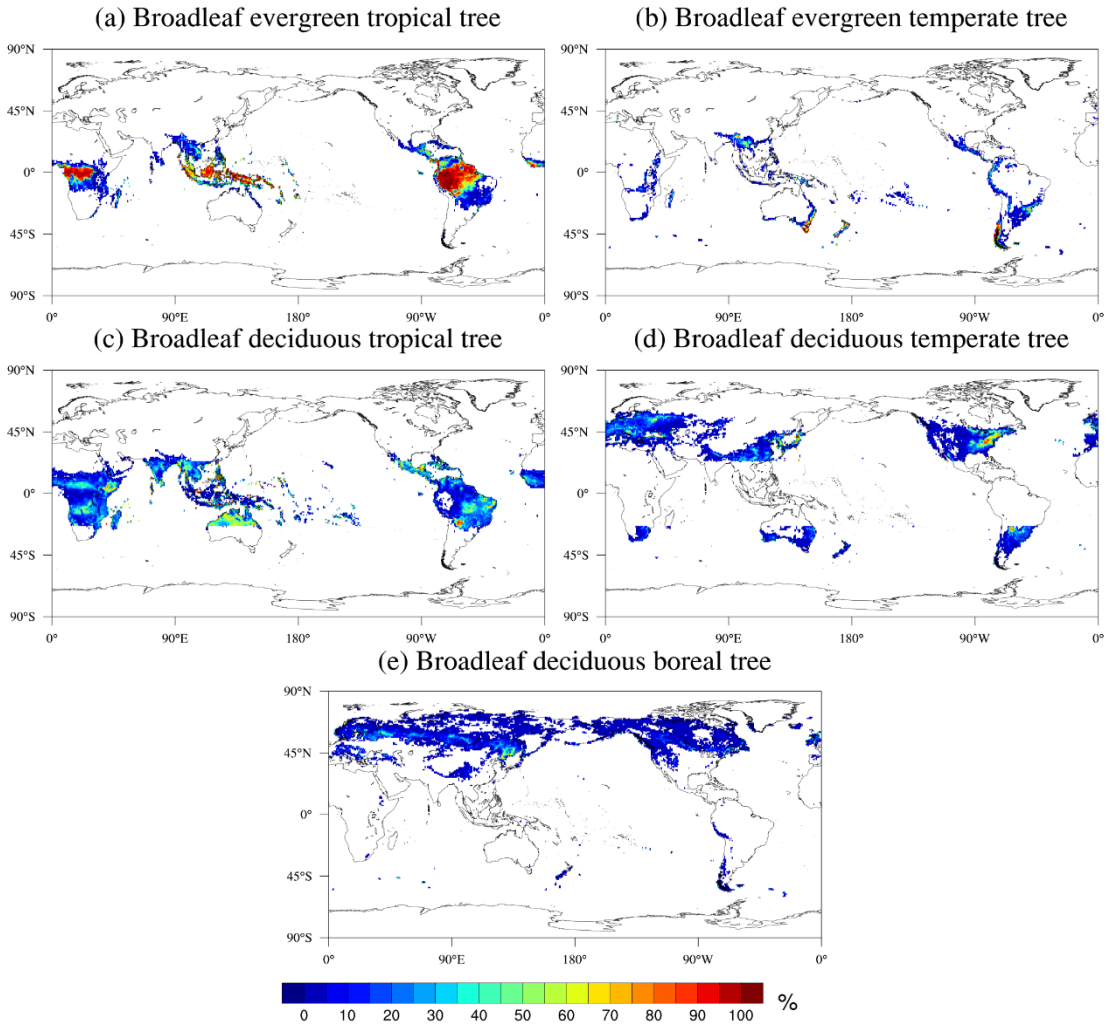

Fig. S3 Spatial distribution of broadleaf trees (%) based on the plant type functions used in global models.

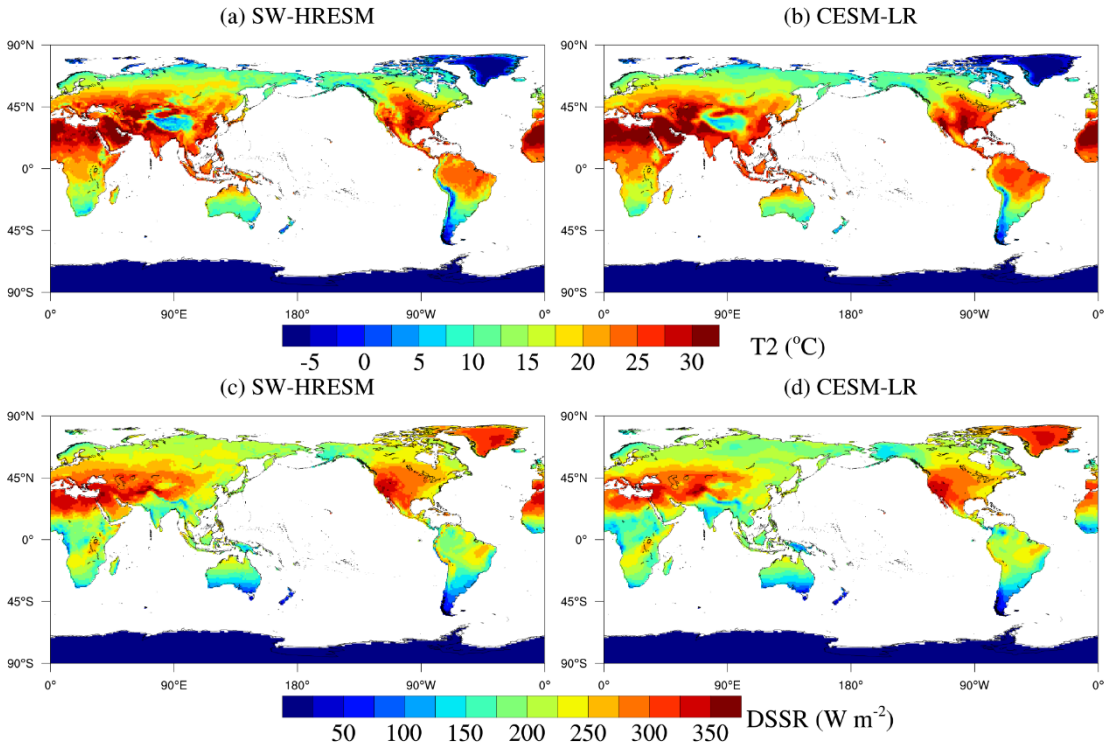

Fig. S4 Spatial distribution of 2-m air temperature and downward surface solar radiation. Shown are results based on SW-HRESM and CESM-LR simulations during the summer of 2015-2019

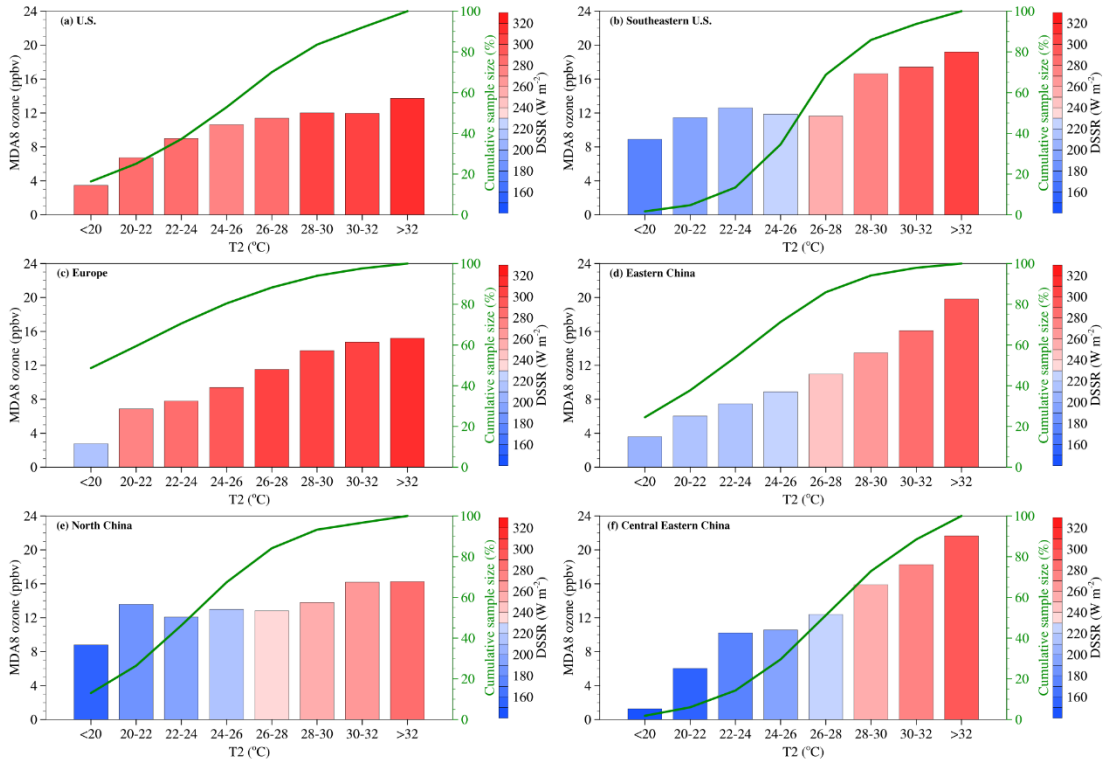

Fig. S5 The contribution of biogenic volatile organic compound emissions to ozone. Shown are results along 2-m air temperature, with shaded color representing downward surface solar radiation (DSSR) over six regions during the summers of 2015-2019. The cumulative sample size over temperature bins is shown in the solid green line.

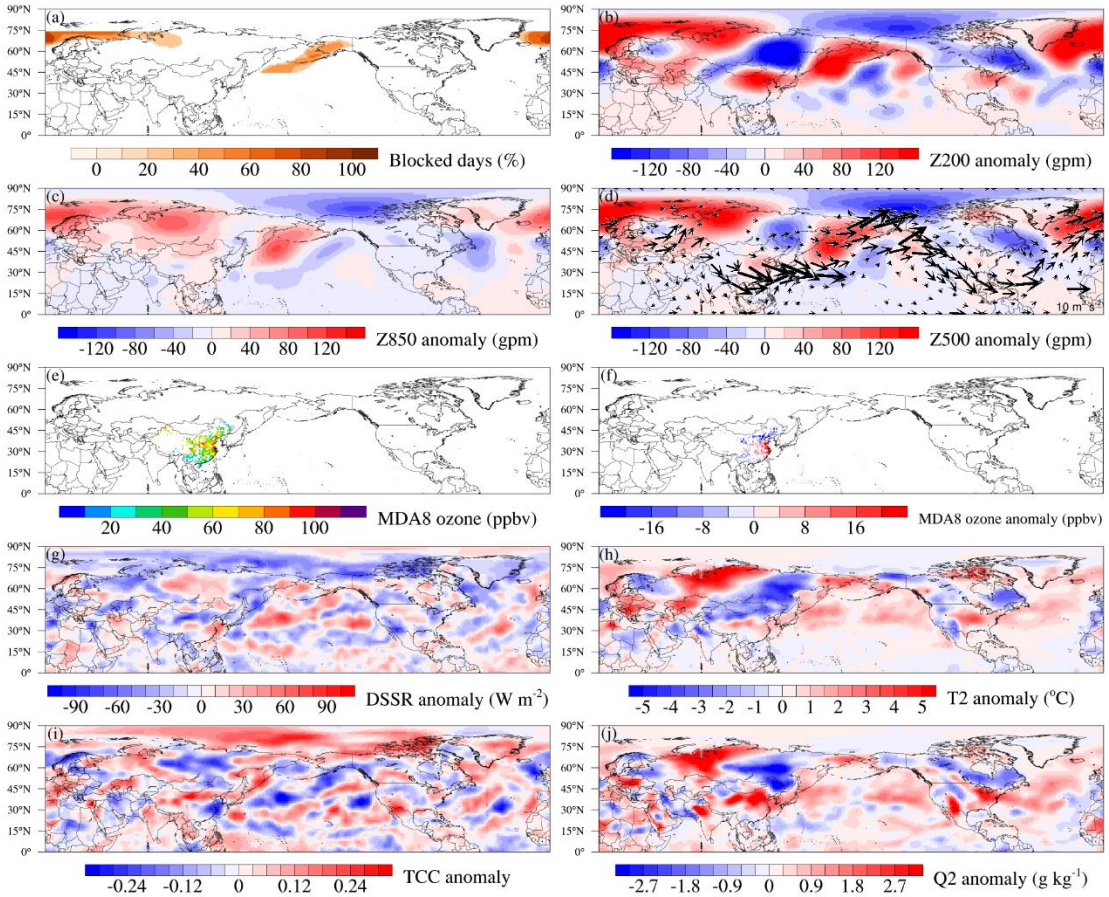

Fig. S6 Spatial distribution of blocking, ozone and geopotential height. Shown are results of anomalies of geopotential height at (b), 200 hPa, (c) 850 hPa, (d) 500 hPa, (e) ozone concentrations, anomalies of (f) ozone, (g), DSSR, (h) 2-m air temperature, (i) total cloud cover and (j) 2-m specific humidity. The results are composited during a specific blocking event over Euro-Atlantic region.

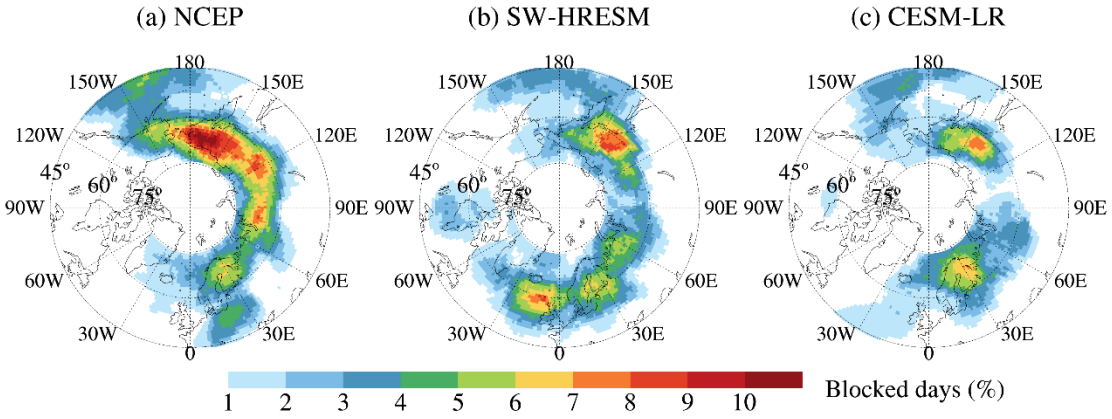

Fig. S7 Mean ratio of atmospheric blocking days based on SW-HRESM and CESM-LR simulations and NCEP reanalysis data during the summer of 2015-2019.

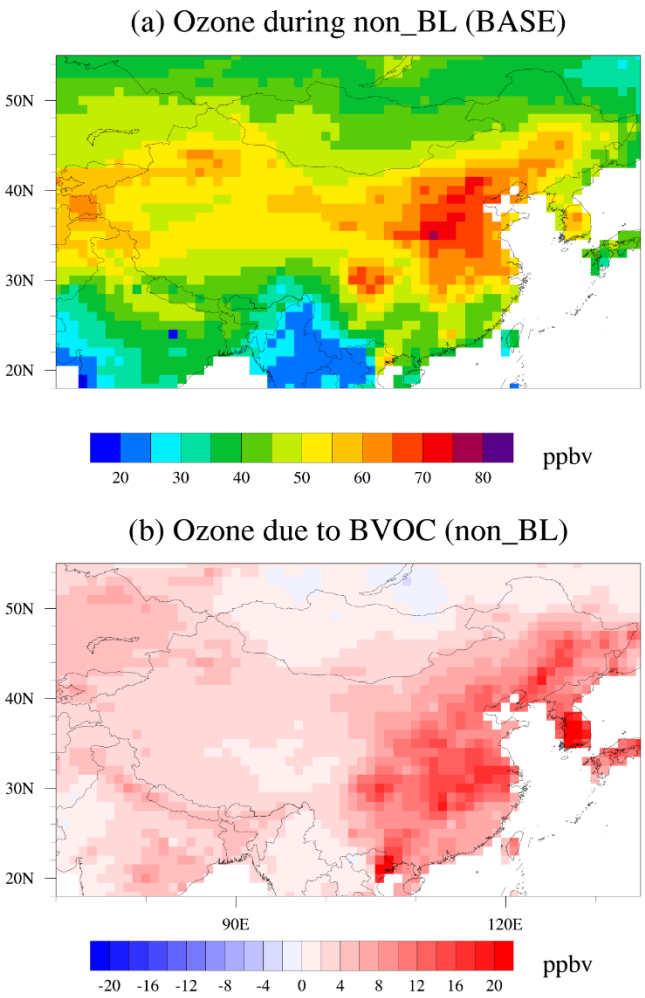

Fig. S8 Spatial distributions of ozone concentrations. Shown are results during non-blocking for (a) BASE and (b) effect of BVOC emissions.

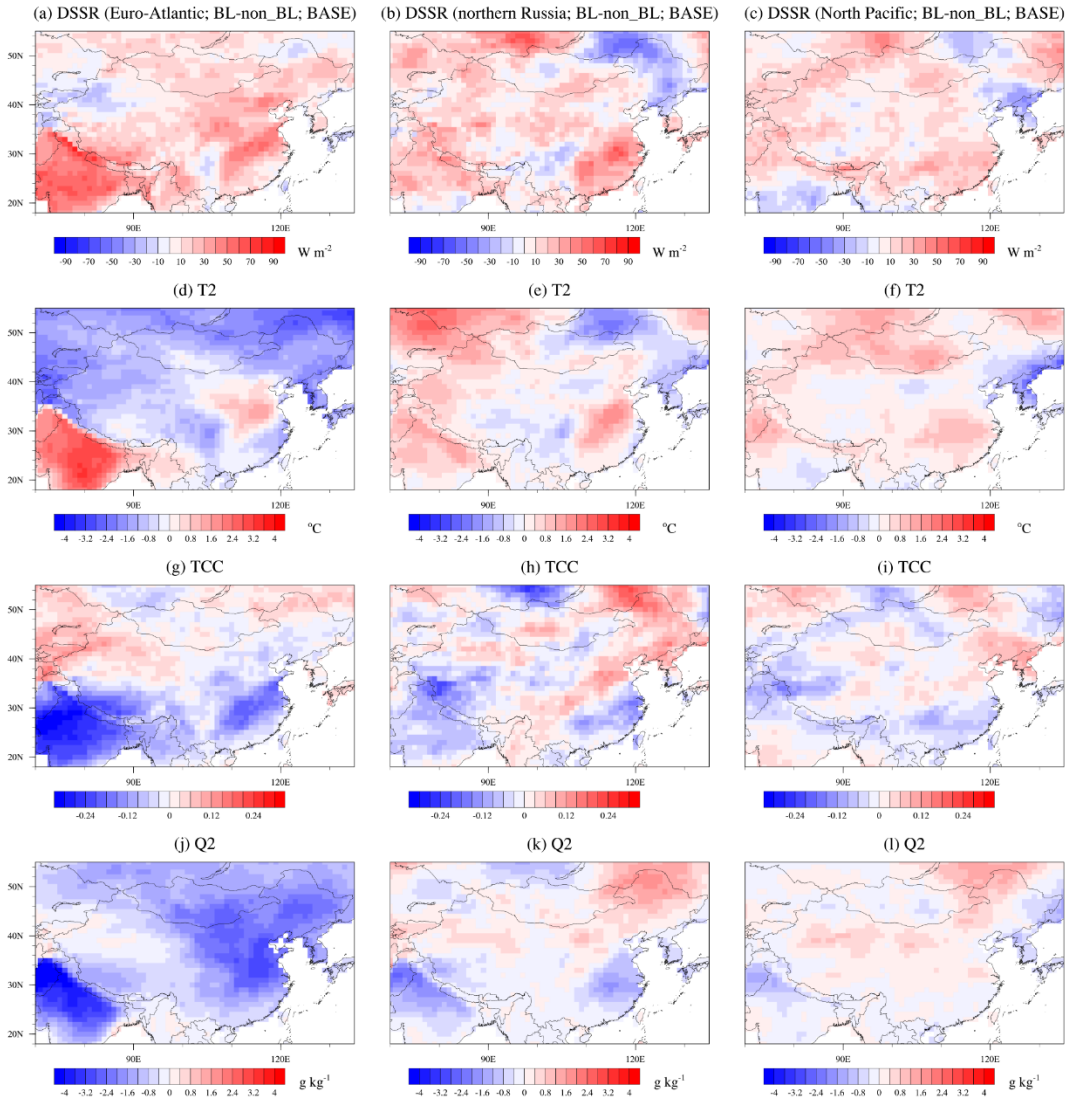

Fig. S9 Spatial distribution of meteorological conditions. Shown are the differences in DSSR (top row), 2-m air temperature (second row), total cloud cover (third row) and 2-m specific humidity (bottom row) during blocking events over Euro-Atlantic (left column), northern Russia (middle column) and the North Pacific (right column) compared to non-blocking periods.

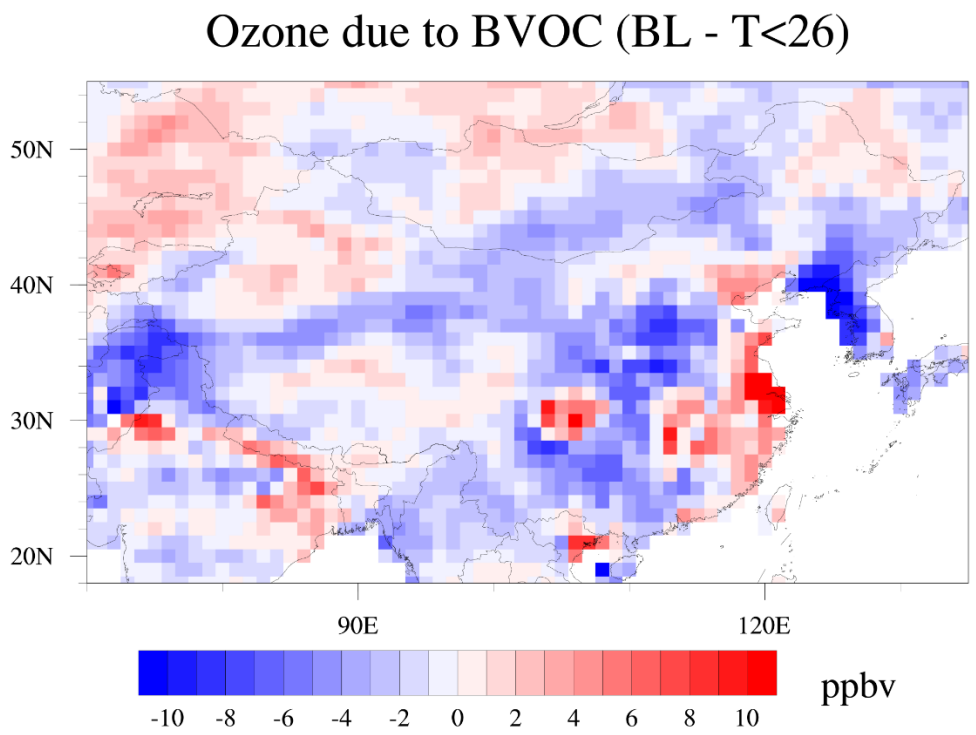

Fig. S10 Spatial distributions of ozone concentrations. Shown are results of the differences in the effects of BVOC emissions on ozone during blocking events over northern Russia, compared to periods with 2-m air temperature below 26 ˚C.

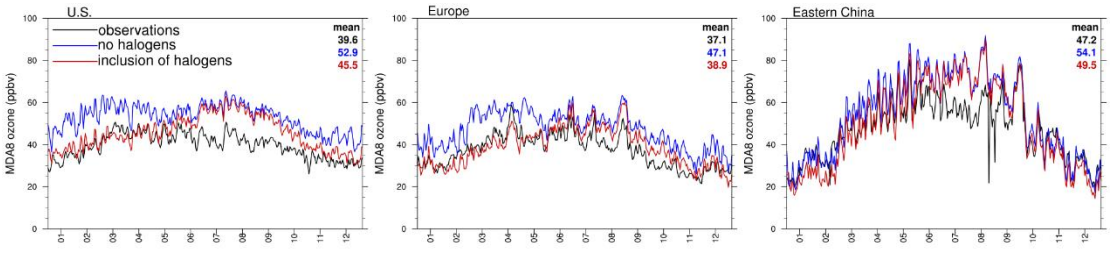

Fig. S11 Evaluation of MDA8 ozone in 2019. Shown are results for the U.S., Europe, and Eastern China using CESM2.2 simulations: comparison of cases with and without halogen chemistry

Reference:
Weng, H., Lin, J., Martin, R., Millet, D. B., Jaeglé, L., Ridley, D., Keller, C., Li, C., Du, M., and Meng, J.: Global high-resolution emissions of soil NOx, sea salt aerosols, and biogenic volatile organic compounds, Scientific Data, 7, 148, 10.1038/s41597-020-0488-5, 2020.